working in the potential region where the film is not active toward the substrate employed.

When the electrocatalyst employed (first coating) is very efficient, i_S can be evaluated by using eq 7 (i_K is large and the third term can be neglected). Then quantities i_A and i_L are obtained from the limiting currents of the current-potential curves recorded with single- and double-coated electrodes (Figure 4). In the case where the electrocatalyst is not able to generate a diffusion-controlled current (Levich current), the system should be analyzed in terms of Koutecky-Levich plots (Figure 5), where the difference of the intercepts of the parallel plots is a direct measure in $1/i_S$.

The high diffusion current found for iron ions in the [Ru(bpy)$_2$Cl(PVP)]Cl fim is of interest. We believe that the uncoordinated protonated pyridine groups at the polymer backbone play an important role for the polymer to achieve this property. However, we can not exclude contributions from porosity.

Acknowledgment. This project was supported by the Swiss National Science Foundation (Grant 2.915-0.85). We thank Drs. J. F. Equey and K. Mueller from our institute and Dr. C. P. Andrieux, CNRS, Paris, for helpful discussions, Dr. J. G. Vos, NIHE, Dublin, for providing us with the [Ru(bpy)$_2$Cl(PVP)]Cl polymer, and Maria Mohos for taking the electron microscope picture.

Registry No. Fe, 7439-89-6; HCl, 7647-01-0; 1-hydroxyphenazine, polymerized, 105103-78-4; carbon, 7440-44-0.

Photochemistry of Colloidal Semiconducting Iron Oxide Polymorphs

Jonathan K. Leland and Allen J. Bard*

Department of Chemistry, University of Texas, Austin, Texas 78712 *(Received: November 14, 1986; In Final Form: May 19, 1987)*

Electrochemical charge collection experiments were carried out with different irradiated iron oxide polymorphs (α-Fe_2O_3, α-FeOOH, β-FeOOH, δ-FeOOH, γ-Fe_2O_3, and γ-FeOOH). A model for direct electron transfer from a particle to an electrode is developed to describe the experimental current-potential behavior. The quasi-Fermi level of electrons for the different species, measured by mediated charge collection experiments, was different for each polymorph. The rate of oxalate and sulfite photooxidation, which was used to probe the relative efficiency of photogenerated charge production and transfer, varied by 2 orders of magnitude among the iron oxides. This efficiency did not correlate with particle size (hydrodynamic radius) or band gap.

Introduction

We report photoelectrochemical studies of colloids and particles of different forms of iron oxide. Iron oxides exist in many crystal structures and stoichiometries.[1] Most of these iron oxides have semiconducting properties, but a comparison of them as photocatalysts has not been made. This polymorphism provides a unique opportunity to study the effects of crystal structure on the semiconducting properties. The most common iron oxide, α-Fe_2O_3, has been studied extensively.[2] α-Fe_2O_3 is an n-type semiconductor with a narrow band gap (2.2 eV). The material has a somewhat positive flat-band potential, -0.58 V vs. NHE at pH 12.0[2f] and very low electron and hole mobility, about 10^{-2} cm^2/(V·s).[2a] α-Fe_2O_3 can carry out the photooxidation of H_2O to O_2,[2f-i] although it suffers from instability in acidic solutions and generally poor efficiencies. The only reports on the photochemistry or photoelectrochemistry of iron oxides colloids have been on α-Fe_2O_3.[3] The photoelectrochemical properties of the other iron oxides remain uncharacterized.

There are many naturally occurring and synthetic iron oxides, but not all (e.g., the green rusts and dehydrated gels) have well-defined crystal structures. Transformation of one structure to another is possible by hydration-dehydration and/or partial oxidation-reduction.[1a] Since the most stable form is α-Fe_2O_3, any elevated temperature technique used to prepare solid electrodes (like growth of single crystals from melts or sintering of pressed pellets) by starting with the other iron oxides results in transformation to α-Fe_2O_3. However, colloidal solutions and particulate dispersions of the different iron oxides can be prepared and were used in this study.

Numerous experimental techniques have been used to study the photoelectrochemistry of colloids and compare their behavior to that of solid semiconductor electrodes of the same material.[3e,4,5]

(1) (a) Bernal, J. D.; Dasgupta, D. R.; MacKay, A. L. *Clay Miner. Bull.* **1959**, *4*, 15. (b) Murray, J. W. In *Marine Minerals*; Burns, R. G., Ed.; Mineralogical Society of American: Washington, DC, 1979; Chapter 2, p 47. (c) Lindsley, D. H. *Rev. Mineral.* **1976**, *3*, 1. (d) Gallagher, K. J. *Nature (London)* **1970**, *226*, 1225. (e) Chukhrov, F. V. *Int. Geol. Rev.* **1973**, *19*, 873. (f) Okamoto, S. *J. Am. Ceram. Soc.* **1968**, *51*, 594.

(2) (a) Morin, F. J. *Phys. Rev.* **1954**, *93*, 1195. (b) Gardner, R. F. G.; Sweett, F.; Turner, D. W. *J. Phys. Chem. Solids* **1963**, *24*, 1175. (c) Lewis, D. C.; Westwood, W. D. *Can. J. Phys.* **1964**, *42*, 2367. (d) Bailey, P. C. *J. Appl. Phys.* **1960**, *31*, 39S. (e) Wickersheim, K. A.; Lefever, R. A. *J. Chem. Phys.* **1962**, *36*, 844. (f) Quinn, R. K.; Nasby, R. D.; Baughman, R. J. *Mater. Res. Bull.* **1976**, *11*, 1011. (g) Kennedy, J. H.; Frese, K. W., Jr. *J. Electrochem. Soc.* **1978**, *125*, 709. (h) Turner, J. E.; Hendewerk, M.; Parameter, J.; Neiman, D.; Somorjai, G. A. *J. Electrochem. Soc.* **1984**, *131*, 1777. (i) Hardee, K. L.; Bard, A. J. *J. Electrochem. Soc.* **1976**, *123*, 1024. (j) Dare-Edwards, M. P.; Goodenough, J. B.; Hamnett, A.; Trevellick, P. R. *J. Chem. Soc., Faraday Trans. 1* **1983**, *79*, 2027. (k) Kennedy, J. H.; Frese, K. W., Jr. *J. Electrochem. Soc.* **1978**, *125*, 723. (l) Hardee, K. L.; Bard, A. J. *J. Electrochem. Soc.* **1977**, *124*, 215. (m) Shinar, R.; Kennedy, J. H. *J. Electrochem. Soc.* **1983**, *130*, 860. (n) Kennedy, J. H.; Shinar, R.; Ziegler, J. P. *J. Electrochem. Soc.* **1980**, *127*, 2307. (o) Sammells, A. F.; Ang, P. G. P. *J. Electrochem. Soc.* **1979**, *126*, 1831. (p) Yeh, L.-S. R.; Hackerman, N. *J. Electrochem. Soc.* **1977**, *124*, 833. (q) Wilhelm, S. M.; Yun, K. S.; Ballenger, L. W.; Hackerman, N. *J. Electrochem. Soc.* **1979**, *126*, 419. (r) Curran, J. S.; Gissler, W. G. *J. Electrochem. Soc.* **1979**, *126*, 56. (s) Iwanski, P.; Curran, J. S.; Gissler, W.; Memming, R. *J. Electrochem. Soc.* **1981**, *128*, 2128. (t) Frese, K. W.; Kennedy, J. H. *Extended Abstracts*, 153rd Meeting of the Electrochemical Society, Seattle, WA; Electrochemical Society: Pennington, NJ, 1983.

(3) (a) Moser, J.; Grätzel, M. *Helv. Chim. Acta* **1982**, *65*, 1436. (b) Grätzel, M.; Kiwi, J.; Morrison, C. L.; Davidson, R. S.; Tseung, A. C. C. *J. Chem. Soc., Faraday Trans. 1* **1985**, *81*, 1883. (c) Haupt, J.; Peretti, J.; Van Steenwikel, R. *Nouv. J. Chim.* **1984**, *8*, 633. (d) Herrmann, J. M.; Mozzanega, M. N.; Pichat, P. *J. Photochem.* **1983**, *22*, 333. (e) Dimitrijević, N. M.; Savić, D.; Mičić, O. I.; Nozik, a. J. *J. Phys. Chem.* **1984**, *88*, 4278.

(4) (a) White, J. R.; Bard, A. J. *J. Phys. Chem.* **1985**, *89*, 1947. (b) Ward, M. D.; White, J. R.; Bard, A. J. *J. Am. Chem. Soc.* **1983**, *105*, 27. (c) Bard, A. J.; Pruiksma, R.; White, J. R.; Dunn, W.; Ward, M. D. *Proc. Electrochem. Soc.* **1982**, *82-3*, 381. (d) Ward, M. D.; Bard, A. J. *J. Phys. Chem.* **1982**, *86*, 3599. (e) Dunn, W. W.; Aikawa, Y.; Bard, A. J. *J. Am. Chem. Soc.* **1981**, *103*, 3456. (f) Dunn, W. W.; Aikawa, Y.; Bard, A. J. *J. Electrochem. Soc.* **1981**, *128*, 222.

0022-3654/87/2091-5076$01.50/0

TABLE I: Energetic and Kinetic Data for Different Iron Oxide Polymorphs[a]

iron oxide	d, μm	nE_F*	k^0, cm/s	$k^{0,b}$ cm/s	k_{OX}, s^{-1}	k_{SO}, s^{-1}	BG, eV	N_{CB}, cm^{-3}
α-Fe_2O_3	0.14 (10.2)[c]	−0.52	3.7×10^{-8}	3.7×10^{-8}	1.2×10^{-4}	42×10^{-4}	2.02	2.0×10^{17}
γ-Fe_2O_3	0.39	+0.02	1.0×10^{-7}	1.1×10^{-9}	17.3×10^{-4}	25×10^{-4}	2.03	2.0×10^{17}
δ-FeOOH	0.19	+0.33	5.5×10^{-6}	7.0×10^{-12}	4.6×10^{-4}	6.0×10^{-4}	1.94	2.5×10^{17}
β-FeOOH	0.19 (56.5)[c]	+0.54	2.5×10^{-4}	4.1×10^{-10}	0.41×10^{-4}	4.4×10^{-4}	2.12	4.0×10^{17}
γ-FeOOH	0.37	+0.41	5.7×10^{-6}	7.7×10^{-12}	12.0×10^{-4}	52×10^{-4}	2.06	1.8×10^{17}
α-FeOOH	0.17	−0.16	6.0×10^{-9}	2.9×10^{-11}	2.5×10^{-4}	2.7×10^{-4}	2.10	3.3×10^{17}
FeO_x·SiO_2	0.32 (273)[c]		4.0×10^{-8}	4.0×10^{-8}		20×10^{-4}		1.4×10^{17}
Pt/α-Fe_2O_3			1.0×10^{-5}	1.0×10^{-5}				2.0×10^{17}
α-Fe_2O_3 (single crystal)		−0.58[d]						
α-Fe_2O_3 (polycrystalline)		−0.52[e]						

[a] Values for d, hydrodynamic diameter; nE_F*, quasi-Fermi level for electrons, vs. SCE at pH 12.0; k^0, standard heterogeneous rate constant for electron transfer; k_{OX}, pseudo-first-order rate constant for oxalate oxidation; k_{SO}, pseudo-first-order rate constant for sulfite oxidation; BG, band gap; and N_{CB}, steady-state concentration of electrons. [b] Overpotential referenced to −0.52 V vs. SCE at pH 12.0. [c] BET surface area, m^2/g. [d] V_{FB} taken from ref 2f. [e] V_{FB} taken from ref 2k,q.

Kinetic models have also been proposed on the basis of photogeneration of electron–hole (e^-h^+) pairs, bulk and interfacial kinetics, and mass transport to describe the reaction rates.[5d,k,6] Unfortunately, because of the complexity of the processes, experimental verification of these models is often difficult without simplifications, such as the assumption of first-order e^-h^+ recombination kinetics. In this study, charge collection experiments were performed on the irradiated iron oxides with well-defined crystal structures: α- and γ-Fe_2O_3 and α-, β-, γ-, and δ-FeOOH. The effect of potential of the charge collecting electrode was investigated, and Tafel-like plots (e.g., a linear relationship between the logarithm of steady-state photocurrent and overpotential) were found. A model for direct transfer of photogenerated charge from a particle to an electrode was developed to account for this behavior. Mediated charge collection experiments, with a soluble redox couple in solution[4] were also performed to obtain the quasi-Fermi level for electrons under illumination, nE_F*. Information on the relative rate of photogenerated hole reactions was obtained for the photooxidation of oxalate and sulfite.

Experimental Section

All photochemical and photoelectrochemical investigations were carried out by using a 450-W tungsten–halogen lamp, unless stated otherwise. The cell had an optically flat Pyrex window and was thermostated at 25 ± 1 °C. In the charge collection experiments the colloidal solutions were well-stirred and deaerated with purified N_2. Placed in the solution was a platinum flag working electrode, (0.70 cm^2) with its potential measured vs. a saturated calomel reference electrode (SCE). The counter electrode was isolated by means of a glass frit. A potentiostat [Princeton Applied Research (PAR), Princeton, NJ; Model 173] was used to hold the electrode at a constant potential. Photocurrent transients were recorded on an *XYY* recorder (Soltec, Sun Valley, CA; Model 6432).

Sodium tartrate (0.5 M) served as the irreversible hole scavenger in the iron oxide colloidal solution. The pH was adjusted with NaOH or HNO_3. In the mediator experiments either 5 mM $K_3Fe(CN)_6$ or $Ru(NH_3)_6Cl_3$ was used. The effective coulometric cell constant p was measured by controlled potential coulometry of $K_3Fe(CN)_6$ as described previously.[4a] The generation rate of electron–hole (e^-h^+) pairs G was estimated from the photon flux, measured by Reinecke salt [$KCr(NH_3)(NCS)_4$] actinometry[7] and from the known absorbance coefficients of α-Fe_2O_3.[2a,d,e] If we assume that every absorbed photon results in an e^-h^+ pair, G is about 10^{17} e^-h^+ pairs/s.

In the oxalate decomposition experiments, the rate of disappearance of $C_2O_4^{2-}$ was determined by periodically running a cyclic voltammogram at a carbon paste electrode.[8] The anodic peak current (E_p = +1.47 V vs. SCE at pH 2.3) is directly proportional to the concentration of oxalate.[9] The initial concentration of oxalic acid was 5 mM. A PAR Model 175 universal programmer was used in conjunction with the potentiostat to obtain the cyclic voltammograms, which were recorded on an *XY* recorder (Houston Instruments, Austin, TX; Model 2000). The pH was adjusted to 2.3 with HNO_3. Oxygen was bubbled through a presaturator at a flow rate of 200 mL/min before reaching the cell to minimize concentration losses.

In sulfite experiments, the concentration of sulfite was measured by titration with triiodide to a starch end point.[10] The initial concentration of sulfite was 10 mM at pH 4.1 (adjusted with acetate). All other parameters were the same as in the oxalate experiments.

Cyanide concentrations were determined by a potentiometric titration with $AgNO_3$.[11] Iodide concentrations were measured by the same potentiometric titration. Iodine was measured by UV spectroscopy and an amperometric titration.

High-purity α-Fe_2O_3 either was obtained from Puratronics (Alfa Products, Danvers, MA) or was prepared[12a] by mixing an 18 mM solution of $Fe(NO_3)_3$·$9H_2O$ with 46 mM HNO_3. The pH was adjusted to 1.40 with $NaHCO_3$ and the solution held at 100 °C for 24 h in a closed glass vessel. β-FeOOH was prepared[12] by heating a 270 mM solution of $FeCl_3$·$6H_2O$ in 10 mM HCl for 3 days at 90 °C in a closed glass vessel. δ-FeOOH was prepared[1f] by adding $FeSO_4$·$7H_2O$ to 10 M NaOH from which oxygen was rigorously excluded. A light gray precipitate of $Fe(OH)_2$ was formed. To this H_2O_2 was rapidly added, and oxidation occurred with δ-FeOOH formation. (Note: This last step should be carried out with great care and the necessary safety precautions.) The colloids were purified by dialysis (cellulose acetate membrane) and centrifugation. α,γ-FeOOH and γ-Fe_2O_3 were obtained from Dr. H. Hartman. Suspensions were prepared by sonicating 62.5 mg of the dry powder for 15 min in 25 mL of triply distilled water.

Monolayer iron oxide on silica (FeO_x/SiO_2) was prepared by a controlled hydrolysis technique. SiO_2 (Degussa), which was dried at 140 °C overnight, was suspended in doubly distilled (from KOH, followed by CaO under N_2) pyridine. To this mixture anhydrous $FeCl_3$ (prepared by azeotropic distillation from

(5) (a) Moser, J.; Grätzel, M. *J. Am. Chem. Soc.* **1983**, *105*, 6547. (b) Grätzel, M.; Frank, A. J. *J. Phys. Chem.* **1982**, *86*, 2964. (c) Duonghong, D.; Ramsden, J.; Grätzel, M. *J. Am. Chem. Soc.* **1982**, *104*, 2977. (d) Albery, W. J.; Bartlett, P. N.; Porter, J. D. *J. Electrochem. Soc.* **1984**, *131*, 2892, 2896. (e) Jaegar, C. D.; Bard, A. J. *J. Phys. Chem.* **1979**, *83*, 3146. (f) Harbour, J. R.; Hair, M. L. *J. Phys. Chem.* **1979**, *83*, 652. (g) Henglein, A.; Lilie, J. *J. Am. Chem. Soc.* **1981**, *103*, 1059. (h) Rossetti, R.; Brus, L. *J. Phys. Chem.* **1982**, *86*, 4470. (i) Henglein, A.; *Ber. Bunsenges. Phys. Chem.* **1982**, *86*, 241. (j) Becker, W.; Bard, A. J. *J. Phys. Chem.* **1983**, *87*, 4888. (k) Albery, W. J. *J. Chem. Soc., Faraday Trans. 1* **1985**, *81*, 1999. (l) Manassen, J. *Isr. J. Chem.* **1982**, *22*, 190. (m) Brown, J. D.; Williamson, D. L.; Nozik, A. J. *J. Phys. Chem.* **1985**, *89*, 3076.

(6) (a) Curran, J. S.; Lamouche, D. *J. Phys. Chem.* **1983**, *87*, 5405. (b) Gerischer, H. *J. Phys. Chem.* **1984**, *88*, 6096. (c) Hodes, G.; Grätzel, M. *Nouv. J. Chim.* **1984**, *8*, 509.

(7) Wegner, E. E.; Adamson, A. W.; *J. Am. Chem. Soc.* **1966**, *88*, 394.

(8) Adams, R. N. *Electrochemistry of Solid Electrodes*; Marcel Dekker: New York, 1969.

(9) Thrivikraman, K. V.; Keller, R. W.; Wolfson, S. K.; Yao, S. J.; Morgenlander, J. C. *Bioelectrochem. Bioenerg.* **1982**, *9*, 357.

(10) Skoog, D. A.; West, D. M. *Fundamentals of Analytical Chemistry*; Holt, Rinehart, and Winston: New York, 1976.

(11) Kolthoff, I. M.; Furman, N. H. *Potentiometric Titrations*; Wiley: New York, 1931.

(12) (a) Matijevic, E.; Scheiner, P. *J. Colloid Interface Sci.* **1978**, *63*, 509. (b) Matijevic, E. *Pure Appl. Chem.* **1978**, *50*, 1193.

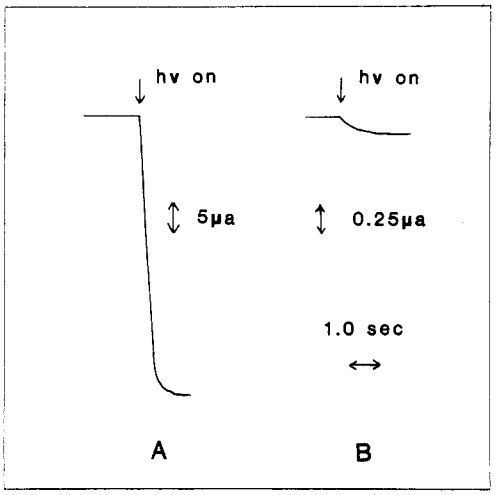

Figure 1. (A) Photocurrent transient with $Ru(NH_3)_6Cl_3$ as mediator for α-Fe_2O_3/tartrate at pH 9.3. (B) Photocurrent transient for direct electron transfer for α-Fe_2O_3/tartrate at pH 9.3 and an electrode potential of 0.55 V. vs. SCE.

benzene) in pyridine was added. The reaction mixture was refluxed under N_2 with rigorous exclusion of moisture for 2 days. After that time the mixture was filtered and washed with copious quantities of pyridine, followed by benzene. The filtrate was dried at 80 °C overnight. To complete the hydrolysis, the solid was suspended in distilled water, centrifuged, and decanted, followed by repetitions of this washing procedure. The slurry was then dialyzed for 4 days (cellulose acetate) and dried. The hydrodynamic diameter and BET surface area for FeO_x/SiO_2 is given in Table I and was approximately the same as that for pure SiO_2. X-ray diffraction shows no peaks for iron oxide. The material is light brown in solid form. Platinized α-Fe_2O_3 was prepared by mixing 500 mg of α-Fe_2O_3 with 4 mL of 0.1 M H_2PtCl_6. This solution was illuminated for 12 h under N_2 and stirring.

The structures of the iron oxides were verified by powder X-ray diffraction using a General Electric Model XRD-6 with Cu $K_{\alpha 1}$ line radiation (ASTM no. 24-81 for γ-Fe_2O_3, 29-713 for α-FeOOH, 13-534 for α-Fe_2O_3, 8-98 for γ-FeOOH, 13-87 for δ-FeOOH, and 13-157 for β-FeOOH). All chemicals were of reagent grade.

The hydrodynamic diameters of the particles were measured by photon correlation spectroscopy (PCS).[13] An Ar ion laser at 514 nm was used. The scattered light pulses were collected with a photomultiplier and fed into a pulse-width discriminator. The data was correlated by a BIC 2020 real-time multibit correlator and analyzed with an Intecolor 3600 microcomputer (Intelligent Systems Corp.). The BET surface area measurements were performed on a Micrometrics Surface Area Analyzer Model 2200. The band gaps were measured by photoacoustic spectroscopy using the experimental configuration described earlier.[14]

Results and Discussion

Photocurrent Measurements with Mediator: Estimation of Conduction Band Energy. Previous studies of irradiated colloids in the presence of a reductant that is irreversibly oxidized by the photogenerated hole and a mediator O capable of accepting a photogenerated electron to produce a species R, which can be oxidized at a collector electrode, have appeared.[4] From the formal potential of the mediator redox couple $E^{\circ\prime}$ and variation of the band energetics of the semiconductor particles through changes in pH, an estimate of the quasi-Fermi level for electrons nE_F^* can be obtained. Such mediated photocurrent measurements were undertaken with the iron oxide colloids, with $Fe(CN)_6^{3-}$ and $Ru(NH_3)_6^{3+}$ as electron acceptors. A typical photocurrent transient for α-Fe_2O_3 in the presence of tartrate as an h^+ acceptor and $Ru(NH_3)_6^{3+}$ as an e^- acceptor is shown in Figure 1. As seen in previous studies with other semiconductors, the photocurrent in the presence of a mediator is much larger than that for direct electron transfer (et) from an irradiated particle to a collector electrode; a photocurrent transient without an acceptor is shown in Figure 1B. Such transients are discussed in a later section. In mediated et studies, the potential of the collector electrode was held 150 mV positive of the anodic peak potential ($E_{p,a}$) for mediator oxidation. The current is the result of the oxidation of $Fe(CN)_6^{4-}$ or $Ru(NH_3)_6^{2+}$ formed at the semiconductor particles at the collector electrode. Current resulting from direct electron transfer from the particle to the electrode is negligible at this potential, since as shown below with the unmediated systems, a very large overpotential is required to produce an appreciable photocurrent under these conditions. Reaction of the photogenerated hole with the reduced form of the mediator was assumed to be negligible, since the concentration of hole scavenger (tartrate) was 100 times larger than that of the mediator.

Through this type of experiment, the quasi-Fermi level for electrons, nE_F^*, is determined. At equilibrium under illumination the difference between nE_F^* and the standard reduction potential, $E^{\circ\prime}$, of the mediator will dictate the final ratio of oxidized mediator C_O^{eq} to reduced mediator C_R^{eq} through the Nerst equation:

$$E^{\circ\prime} - nE_F^* = 0.0591 \log (C_R^{eq}/C_O^{eq}) \quad (1)$$

For most oxide semiconductors nE_F^* changes about 59 mV per unit pH change:[15]

$$nE_F^* = nE_F^*(\text{pH } 0) - 0.0591(\text{pH}) \quad (2)$$

Substitution of eq 2 into eq 1 yields

$$\log (C_R^{eq}/C_O^{eq}) = \text{pH} + [E^{\circ\prime} - nE_F^*(\text{pH } 0)]/0.0591 \quad (3)$$

which is valid when $E^{\circ\prime}$ is independent of pH. A plot of log (C_R^{eq}/C_O^{eq}) vs. pH will be linear with a unit slope and an intercept on the pH axis at the pH where $E^{\circ\prime} = nE_F^*$:

$$nE_F^*(\text{pH } 0) - 0.0591(\text{pH}) = E^{\circ\prime} \quad (4)$$

Thus, the nE_F^* at any pH can be determined if the ratio C_R^{eq}/C_O^{eq} and $E^{\circ\prime}$ are known. The bulk concentration of reduced mediator in solution at any time can be related to the current by the expression for a mass-transfer-controlled reaction:[16]

$$C_R = i_{med}/FAm \quad (5)$$

where i_{med} is the current that results from the oxidation of the reduced form of the mediator; i.e., the collector electrode serves as an indicator for C_R. The mass-transfer coefficient m (assumed equal for oxidized and reduced mediator) can be evaluated from the measured effective coulometric cell constant p (s^{-1})[16] and is given by

$$m = pV/A \quad (6)$$

C_O is evaluated from

$$C_O = C^* - C_R \quad (7)$$

where C^* is the total concentration of the mediator in both oxidation states. This can be related to the dark current for the oxidation of the mediator i_{med}^* when the mediator is completely in the reduced form:

$$C^* = i_{med}^*/FAm \quad (8)$$

so that

$$i_{med}/(i_{med}^* - i_{med}) = C_R/C_O \quad (9)$$

Under conditions when the et and mass-transfer kinetics at the semiconductor particle surface are so fast that the ratio C_R/C_O represents the equilibrium ratio, C_R^{eq}/C_O^{eq}, a plot of log $[i_{med}/$

(13) Berne, B. J.; Pecora, R. *Dynamic Light Scattering with Applications to Chemistry, Biology, and Physics*; Wiley Interscience: New York, 1976.
(14) Gray, R. C.; Fishman, V. A.; Bard, A. J. *Anal. Chem.* **1977**, *49*, 697.
(15) (a) Scaife, D. E. *Sol. Energy* **1980**, *25*, 41. (b) Butler, M. A.; Ginley, D. S. *J. Electrochem. Soc.* **1978**, *125*, 228. (c) Nozik, A. J. *Annu. Rev. Phys. Chem.* **1978**, *29*, 189.
(16) Bard, A. J.; Faulkner, L. R. *Electrochemical Methods*; Wiley Interscience: New York, 1980.

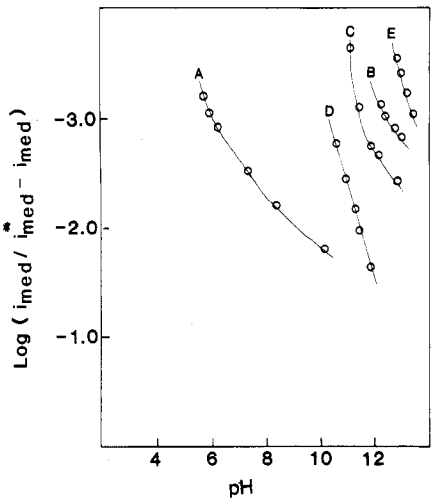

Figure 2. Log $[i_{med}/(i_{med}^* - i_{med})]$ vs. pH behavior with $K_3Fe(CN)_6$ as mediator for (A) γ-Fe_2O_3, (B) β-FeOOH, (C) δ-FeOOH, (D) α-FeOOH, and (E) γ-FeOOH.

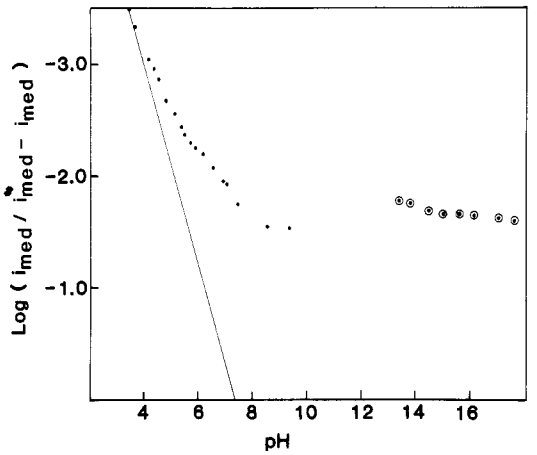

Figure 3. Log $[i_{med}/(i_{med}^* - i_{med})]$ vs. pH behavior for α-Fe_2O_3 using $K_3Fe(CN)_6$ (open circles) and $Ru(NH_3)_6Cl_3$ (closed circles) as mediators. The difference in $E^{\circ\prime}$ for $K_3Fe(CN)_6$ and $Ru(NH_3)_6Cl_3$ was, for comparison purposes, corrected by adjusting the pH scale 1 unit for every 59 mV; see eq 3.

$(i_{med}^* - i_{med})]$ vs. pH for the illuminated iron oxide dispersions with $Fe(CN)_6^{3-/4-}$ or $Ru(NH_3)_6^{3+/2+}$ as mediators can be used to determine nE_F^*. Typical plots are shown in Figures 2 and 3. The plots only approach the theoretical slope of unity at the lower pH values and for low (<0.1–1%) conversions of O to R. A careful set of measurements with α-Fe_2O_3 and both mediators over a wide pH range is shown in Figure 3. The $E^{\circ\prime}$ values for the $Fe(CN)_6^{3-/4-}$ and $Ru(NH_3)_6^{3+/2+}$ couples were 0.22 and −0.24 V vs. SCE (as measured by cyclic voltammetry). The value of nE_F^* was estimated by extrapolation of the two lowest points obtained with $Ru(NH_3)_6^{3+}$ (slope 0.90). The $Fe(CN)_6^{3-/4-}$ data were plotted on the same axes by correcting for the difference in $E^{\circ\prime}$ values with respect to nE_F^*(pH 0) (see eq 3). The log $[i_{med}/(i_{med}^* - i_{med})]$ behavior does not follow a straight line but is curved and eventually flattens out. The behavior appears to become more ideal as the pH decreases. At high pH's the line flattens out and the ratio of the steady-state (ss) concentrations C_R^{ss}/C_O^{ss} becomes insensitive to pH changes. We might also note that for α-Fe_2O_3 colloids the flat-band potential V_{FB} may not vary by 59 mV/pH unit. Dimitrijevic et al.,[3e] using pulse radiolysis techniques, found only a 10-mV change/pH unit.

The deviation from ideality in our experiments demonstrates that the photoreduction of $Ru(NH_3)_6Cl_3$ and $K_3Fe(CN)_6$ by iron oxide particles is kinetically controlled and the equilibrium ratio of C_R to C_O cannot be reached under illumination as predicted by the Nernst equation. The slow approach to equilibrium is probably due to a small standard heterogeneous rate constant for et to mediator, k^0 (which is common for semiconductors[6c]), and large e^-h^+ recombination rates.

To obtain the correct value for nE_F^* at any pH, one must extrapolate to that pH from the region where the slope of the line is 1.0. The values of nE_F^* for all the iron oxides, extrapolated to pH 12.0, are listed in Table I. One explanation of the large differences in nE_F^* for the different iron oxides involves a significant contribution from intra-band-gap states (or surface states). If these mediate electron transfer instead of the conduction band level, the intra-band-gap-state energy would be measured. The presence of surface states on CdS particles has been inferred by measurements of the type performed here[17] and from luminescence experiments.[5h] Kennedy and Frese, using a polycrystalline α-Fe_2O_3 electrode, reported the presence of bulk states 0.6 eV below the conduction band.[2k] The value of nE_F^* obtained for α-Fe_2O_3 agrees with the values of the V_{FB} reported in the literature for single-crystal[2f] and polycrystalline[2k,g] α-Fe_2O_3 (Table I) and suggests that the proposed method of examining semiconductor powders is a reasonable one. Note, however, that the value of V_{FB} for α-Fe_2O_3 is somewhat dependent on the method of preparation.[2q] An estimate of the values of the potentials for the CB (conduction band) and VB (valence band) edges at pH 12 determined and those reported can be obtained from the band gap measured by photoacoustic spectroscopy (2.02 eV) and nE_F^* (by assuming nE_F^* is 0.1 eV below the CB). This yields, for α-Fe_2O_3, a CB level of −0.62 V vs. SCE (compared to −0.68 V reported for the single crystal[2f] and −0.92 V for polycrystalline[2k,q]) and VB level of +1.40 V (compared to +1.52 V for single crystal and +1.28 V for polycrystalline).

The method developed here for the measurement of nE_F^* from the mediated charge collection techniques differs from those previously described.[4] These other techniques measured the photocurrent initial slope or steady-state photocurrent as a function of pH. The pH for the onset of photocurrent was taken as the point where $nE_F^* \approx E^{\circ\prime}$. While those methods are still applicable, the method described here provides a better estimate of nE_F^*, when equilibrium can be obtained. As will be shown in a forthcoming publication,[18] colloids of WO_3 do follow the behavior predicted by the Nernstian condition.

Direct Electron Transfer. As in experiments with TiO_2 and CdS particles,[4] anodic photocurrents could be obtained at a collector electrode in the absence of a mediator during irradiation of iron oxide colloids in the presence of an irreversible hole scavenger such as tartrate or oxalate ion. A typical photocurrent transient for α-Fe_2O_3 is shown in Figure 1B. Upon illumination a steady-state photocurrent is reached within a fraction of a second. The anodic photocurrent is a result of direct et from the illuminated particle to the electrode.[4c,d] If et from the particles to the electrode were rapid, an anodic photocurrent would appear, when the electrode potential was just positive of nE_F^*; i.e., a relatively low overpotential would be required for et. In this work, we consider the question of the kinetics of et from a particle in solution to an inert electrode. Although our purpose was not to model the overall kinetics of charge generation and transport, recombination, and transfer to hole scavengers, knowledge of these processes is necessary to understand direct et to the electrode.

If the steady-state photocurrent is plotted vs. electrode potential, the behavior shown in Figure 4 for γ-FeOOH is observed. The indicated nE_F^* value is that obtained from mediator experiments. Thus, for iron oxide a large overpotential is required to produce an appreciable photocurrent from the particle (overpotential being defined as the difference between the electrode potential and nE_F^*). Such behavior is indicative of slow heterogeneous electron transfer.[16] The data can be treated by assuming that electron transfer follows that of a totally irreversible electrode reaction. A plot of the logarithm of the photocurrent density vs. electrode potential results in a straight line (Tafel behavior), as shown in

(17) Finlayson, M. F.; Wheeler, B. L.; Kakuta, N.; Park, K.-H.; Bard, A. J.; Campion, A.; Fox, M. A.; Weber, S. E.; White, J. M. *J. Phys. Chem.* **1985**, *89*, 5676.

(18) Leland, J. K.; Bard, A. J., *J. Phys. Chem.*, accompanying paper in this issue.

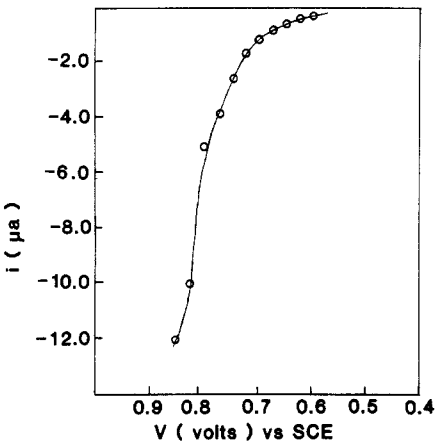

Figure 4. Steady-state photocurrent vs. electrode potential for δ-FeOOH/tartrate at pH 11.3.

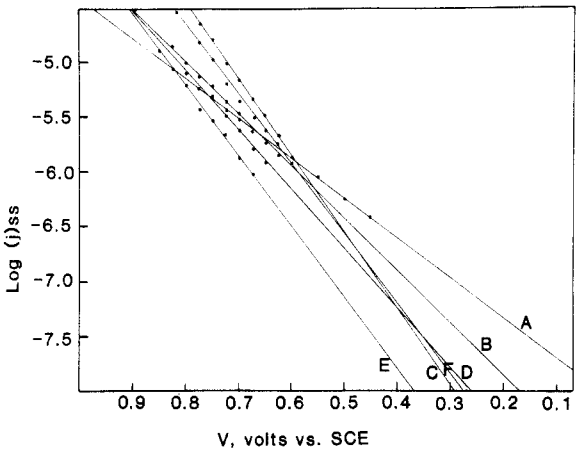

Figure 5. Log j_{ss} vs. electrode potential plots demonstrating the Tafel behavior for all iron oxides: (A) α-Fe_2O_3 at pH 10.3; (B) γ-Fe_2O_3 at pH 11.4; (C) δ-FeOOH at pH 11.3; (D) β-FeOOH at pH 10.6; (E) γ-FeOOH at pH 10.8; (F) α-FeOOH at pH 11.6.

Figure 5. The Tafel slopes deviate from 118 mV, characteristic of a one-electron rate-determining step (n_a = 1) and α = 0.5 process.[16] If n_a = 1, then α, the transfer coefficient for the iron oxides, varies between 0.59 and 0.78. Transfer coefficients for the reduction of methylviologen by TiO_2 colloids have been estimated as 0.52.[5b]

That the direct et process follows Tafel-like behavior suggests that the current–potential behavior for the iron oxides follows Butler–Volmer kinetics, i.e.

$$i_{ss} = nFAN_{CB}k^0 \exp[(1 - \alpha)nf\eta] \qquad (10)$$

or

$$\log j_{ss} = \log (nFN_{CB}k^0) + (1 - \alpha)nf\eta/2.303 \qquad (11)$$

where $j_{ss} = i_{ss}/A$, F is Faraday's constant, A is the electrode area, N_{CB} is a measure of the total concentration of available electrons in the conduction band of all particles at the electrode surface, k^0 is a standard heterogeneous rate constant, f is F/RT, η is overpotential, i_{ss} is the steady-state photocurrent, and j_{ss} is the steady-state photocurrent density. Such an expression can be used to obtain the relative k^0 values for each iron oxide and thus compares relative et kinetics. To estimate the k^0, N_{CB} must be determined; this was done with the following model. First, we assume that the working electrode compartment contains a monodisperse particle system, where the light is uniformly absorbed by each particle and total light absorption by the system is low. Thus, the generation of e^-h^+ pairs by light is constant over the entire particle, and the photochemistry in colloidal solution can be treated in the same way as that in a homogeneous solution.[4a] The solution is so well stirred that the concentration of species at the surface of the electrode does not differ appreciably from

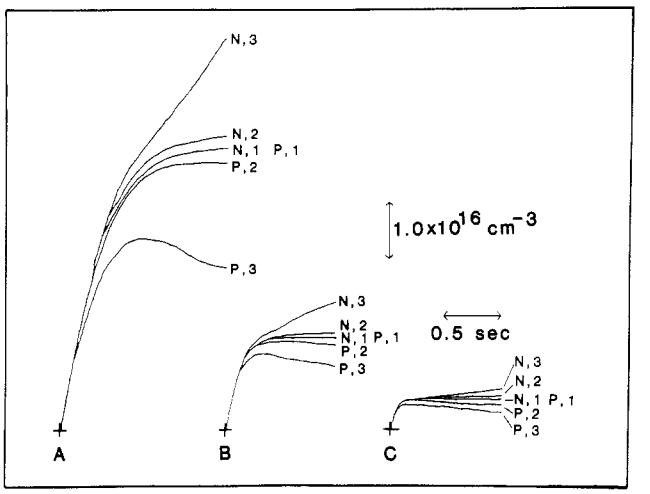

Figure 6. Numerical solutions to eq 12 and 13 for N_{CB}, conduction band electrons, and P_{VB}, valence band holes, with k_r equal to (A) 0.4×10^{-16} $cm^3/[(e^-h^+)\cdot s]$, (B) 0.4×10^{-15}, and (C) 0.4×10^{-14} and k_{OX} equal to (1) 1×10^{-2} s^{-1}, (2) 1×10^{-1}, and (3) 1×10^{0}. $G = 1 \times 10^{17}$ cm^{-3}.

that in the bulk and no mass-transfer limitations are present. Since the area of the electrode is many times smaller than the total surface area of the particles, N_{CB} is not perturbed by charge collection and the working electrode only serves as an indicator electrode. We consider the case where holes are scavenged irreversibly by solution species and electrons accumulate in the particle. The electrode is held at a potential where the rate of the back-reaction, transfer of electrons from the electrode to particle, is negligible.

The continuity equation to predict the average conduction band electron density in solution under illumination is given by

$$dN_{CB}/dt = G - k_r N_{CB} P_{VB} - (A/V)k_f N_{CB} \qquad (12)$$

and the average valence band hole density P_{VB} in solution under illumination is given by

$$dP_{VB}/dt = G - k_r N_{CB} P_{VB} - k_{OX} P_{VB} \qquad (13)$$

where G is the generation rate, t is time, k_r is the bimolecular recombination rate constant, k_f is the et rate constant to the electrode, V is solution volume, and k_{OX} is the pseudo-first-order rate constant for oxidation of the hole scavenger. Numerical solutions to eq 12 and 13 with the et term $(A/V)k_f N_{CB}$ set to zero and with the measured G value yield the results shown in Figure 6. These results show that a steady-state concentration of electrons and holes essentially can be reached for a given k_r, only if k_{OX} is sufficiently small (e.g., $k_{OX} < 1.0 \times 10^{-2}$ s^{-1} for $k_r = 0.4 \times 10^{-16}$ $cm^3/[(e^-h^+)\cdot s]$. If, however, k_{OX} is larger, the particles continuously charge up; i.e., electrons are built up as holes are depleted. Under the conditions where $k_{OX} < 1.0 \times 10^{-2}$ s^{-1}, a change in k_r will influence not only the steady-state N_{CB} (or P_{VB}) but the rate at which steady state is reached (decay constant). By use of a small k_{OX} and adjustment of the decay constant (through k_r) of the numerical solution to match that of the experimental photocurrent transient, a unique fit can be obtained; i.e., the general shape of the numerical solution will match that of the experimental photocurrent transient for only a single pair of k_{OX} and k_r values at a given G (Figure 1). This allows the estimation of N_{CB} and, through eq 11, k^0. These values are listed in Table I. There is a wide variation in k^0 and the values are generally very small, as shown by the large overpotential required to generate a measurable photocurrent. This is consistent with the assumption that at these electrode potentials no significant amount of back-reaction occurs. This also means that, for the iron oxides, direct et will not take place when the electrode potential is near nE_F^*, but only when large overpotentials are employed. Note that these k^0 values pertain to a Pt collector electrode and that different rates of heterogeneous et may be obtained with different electrode materials. The wide variation in k^0 demonstrates that the crystal structure can play an important role in

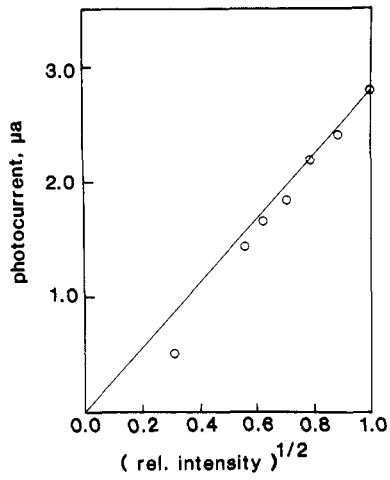

Figure 7. Dependence of the steady-state photocurrent on the square root of the relative light intensity for α-Fe_2O_3/tartrate at pH 7.0. The solid line is the numerical solution with the following parameters: $G = 1 \times 10^{17}$; $k_r = 4 \times 10^{-17}$; $k_{OX} = 1 \times 10^{-2}$. The points are the experimental data; $V = 0.65$ V vs. SCE.

determining the et kinetics, although there are clearly other factors to consider. We do not feel that particle size is an important variable in these measurements, since the k^0 for the different materials varies over several orders of magnitude while the hydrodynamic radius of the particles changes by less than a factor of 3. The mediated charge-transfer experiments have shown that electrons might not necessarily be transferred from the conduction band but through surface states or traps. The difference in the site of et could also account for the variations in k^0. There is also the question concerning the correct potential to use as reference to obtain the overpotential. The k^0 values listed in Table I are derived by referencing the overpotential to the nE_F* measured in the mediated experiments. However, with the exception of α-Fe_2O_3 and possibly α-FeOOH, the et may be occurring through surface states. Another alternative is to reference η (and hence k^0) for all of the iron oxides to the same potential, such as that for α-Fe_2O_3. Such k^0 values, calculated by using–0.52 V vs. SCE at pH 12.0 as the reference potential are also listed in Table I. With this reference level, all of the other iron oxides show much lower values of k^0 than α-Fe_2O_3.

Numerical solutions for the dependence of the steady-state photocurrent on light intensity suggest a square-root dependency, as shown in Figure 7. The experimental data show a reasonable fit to this dependency. Ward et al.[4b] found a linear dependence of the initial photocurrent slope on light intensity with TiO_2 and attributed this to a low recombination rate. The square-root dependence seen here indicates extensive recombination.

The numerical solutions which were fit to experimental photocurrent transients allow an average steady-state electron lifetime to be estimated, where lifetime $\cong 1/k_r P_{ss}$. The values obtained are about 0.5 s (which is also the time constant for the photocurrent transient). The transit time τ for an electron to reach the surface of the particle from the center is calculated by taking μ, the electron mobility for α-Fe_2O_3, to be 10^{-2} $cm^2/(V \cdot s)$:[2a]

$$D/\mu = kT/q \quad (14)$$

and

$$\tau = r^2/\pi^2 D \quad (15)$$

where D is the diffusion coefficient, k is the Boltzmann constant, T is temperature, q is the electronic charge, and r is the particle radius; τ is on the order of 10^{-8} s. If the measured lifetime (ca. 0.5 s) represented the bulk electron lifetime and τ was so much smaller, one would expect photoprocesses on the iron oxide particles to be quite efficient; i.e., photogenerated electrons would have many opportunities of colliding with the particle surface and reacting before recombination. However, the lifetime reported here does not represent a measure of the bulk e^-/h^+ pair lifetime but rather one that represents a surface electron under a special

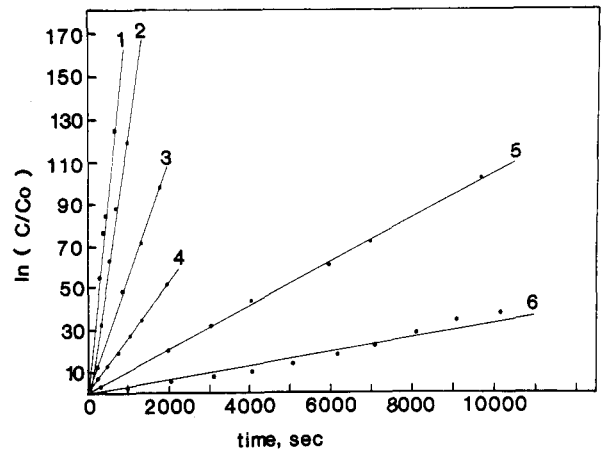

Figure 8. First-order plots for the photodecomposition of oxalate for iron oxides: (1) γ-Fe_2O_3; (2) γ-FeOOH; (3) δ-FeOOH; (4) α-FeOOH; (5) α-Fe_2O_3; (6) β-FeOOH.

set of conditions (at a given G and in the presence of an irreversible hole scavenger). The long surface electron lifetime arises when the photogenerated holes are rapidly removed from the particle surface by tartrate.[5c] Bulk recombination rates are probably much higher, so few electrons generated within the particle reach the surface. Photoelectrophoretic measurements show that TiO_2 particles can retain their negative charge for several minutes.[4e] The measured time constant does not result from mass-transfer (mt) limitations (i.e., particle movement to the electrode surface), since the voltammogram (Figure 4) shows only an exponential rise in the photocurrent with increasing potential and no mt-limited plateau. Grätzel et al.[5c] measured a lifetime of electrons in TiO_2 colloids using methylviologen as a mediator of several milliseconds (with H_2O as a hole scavenger). Frese and Kennedy[2t] measured an electron lifetime using photocurrent transients at various temperatures for α-Fe_2O_3 electrodes; e.g., at 23 °C, it was 16 ms. The mediated charge collection experiments and intensity data suggest that recombination is extensive. The numerical solutions show that, for steady-state conditions, recombination must be many times faster than hole transfer.

In an attempt to increase the rate of et from the iron oxide particles to an electrode (as measured by k^0), the surface of the α-Fe_2O_3 particles was platinized (see Experimental Section). The electrocatalytic properties of platinum are well established.[19] The k^0 was obtained from the Tafel plot of illuminated platinized iron oxide, Pt/α-Fe_2O_3, and is listed in Table I. Platinization increased k^0 by almost 3 orders of magnitude, demonstrating that the k^0 values depend on the surface properties. Dare-Edwards et al.[2j] concluded that, for iron(III) oxide electrodes, the surface properties have a major effect on the photoelectrochemical properties. Sammells and Ang[2o] demonstrated that Pt enhances the photocurrent for iron oxide electrodes. In an attempt to prepare an iron oxide material where surface properties would predominate and bulk recombination effects would be minimized, thin layers of "FeO_x" were deposited on colloidal SiO_2 (see Experimental Section). When this material (FeO_x/SiO_2) was illuminated in the presence of tartrate, electrons could be collected on a Pt electrode, and the observed current again followed a Tafel-type relation. The k^0 for FeO_x/SiO_2 referenced to a potential of –0.52 V vs. SCE is listed in Table I; it is larger than most of the iron oxides but comparable to that for α-Fe_2O_3.

Hole-Transfer Kinetics. To probe the hole-transfer processes of the iron oxides, the rates of photooxidation of several compounds were measured. Several previous studies of photocatalytic processes at α-Fe_2O_3 particles have been reported.[20] Figure 8 is a plot of the decrease in concentration of oxalate in the presence

(19) Pletcher, D. *J. Appl. Electrochem.* **1984**, *14*, 403.
(20) (a) Frank, S. N.; Bard, A. J. *J. Phys. Chem.* **1977**, *81*, 1484. (b) Kraeutler, B.; Bard, A. J. *J. Am. Chem. Soc.* **1978**, *100*, 5985. (c) Hsiao, C. Y.; Lee, C. L.; Ollis, D. F. *J. Catal.* **1983**, *82*, 418. (d) Herrmann, J. M.; Pichat, P. *J. Chem. Soc., Faraday Trans. 1* **1980**, *76*, 1138.

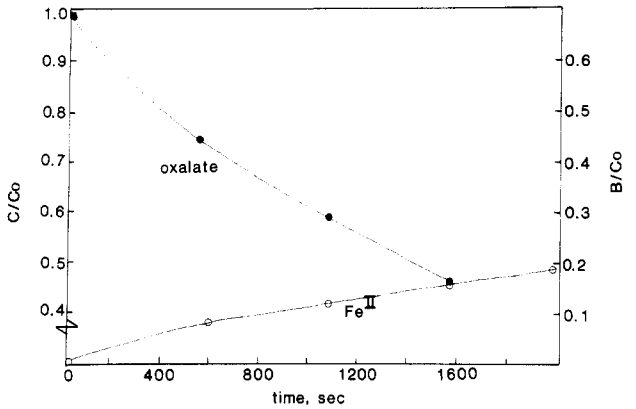

Figure 9. Time dependence of normalized oxalate decomposition (C/C_0) and ferrous ion production (B/C_0) for δ-FeOOH.

of irradiated iron oxides in O_2-saturated solutions. Here photogenerated holes lead to the oxidation of oxalate (ultimately to CO_2), while the electrons cause reduction of oxygen. The reaction appears to follow overall first-order kinetics for removal of oxalate, since a plot of ln (C/C_0) vs. time is linear, where C is the concentration of oxalate and C_0 is its initial concentration. The rate of disappearance of oxalate under identical conditions in the absence of iron oxide is negligible on the time scale of the experiment. From the slope of the lines in Figure 8 pseudo-first-order rate constants can be determined; these are listed in Table I. As seen from this experiment, the rate of oxalate photooxidation varies by a factor of about 30 among the iron oxides. Furthermore, cyclic voltammograms at a carbon paste electrode during the experiments show a wave of 0.20 V vs. SCE that grew with irradiation time. This wave is attributed to the oxidation of ferrous oxalate, which is a product from the reductive photodissolution of the iron oxide particles. Photolysis in the absence of O_2 results in the complete dissolution of the iron oxide particles with concomitant formation of ferrous oxalate. In one experiment with δ-FeOOH, the ferrous ion concentration was monitored spectrophotometrically as the phenanthroline complex simultaneously with the oxalate concentration (Figure 9). Here the ferrous ion dissolution rate was about one-third that of oxalate decomposition.

The photodecomposition of oxalate is best described as a photocatalytic process[15c] because the reaction is thermodynamically downhill ($\Delta G° < 0$). The overall reaction is probably

$$HC_2O_4^- + {}^1/_2O_2 \rightarrow 2CO_2 + OH^- \qquad (16)$$

(If H_2O_2 was produced as a intermediate, this would be rapidly consumed in the presence of $HC_2O_4^-$.) The photogenerated hole is consumed at the iron oxide surface in the oxidation of oxalate, whereas the electron in the conduction band has several fates. The conduction band being comprised of iron-centered orbitals,[2a] e^- will produce an Fe(II) center at the surface of the particle. At a pH of 2.3, especially in the presence of oxalate, Fe(II) could dissolve.[21] Alternatively, the Fe(II) center at the surface could reduce O_2. If the O_2-reduction pathway is slow, some lattice dissolution can occur. Recently, Grätzel et al.[3b] reported the photodissolution of α-Fe_2O_3 in the presence of chloride ions.

The photooxidation of sulfite by iron oxides in O_2-saturated solutions was also found to be first order (Figure 10). The pseudo-first-order rate constants are given in Table I. The oxidation of sulfite in the absence of iron oxide is also plotted in Figure 10. Here we observe that the rate is not negligible, but the rates with the irradiated iron oxides are significantly higher. Like the oxalate system, there is a wide variation in the rates of photooxidation of sulfite with different iron oxides, but the trend is not the same. For example, in both cases γ-FeOOH and γ-Fe_2O_3 show the fastest oxidation, but α-Fe_2O_3 is much better for sulfite than for oxalate relative to the others. Unlike the oxalate systems, no ferrous ion was found in solution after photolysis of sulfite

(21) Pourbaix, M. *Atlas of Electrochemical Equilibria in Aqueous Solutions*; Pergamon: Brussels, 1966.

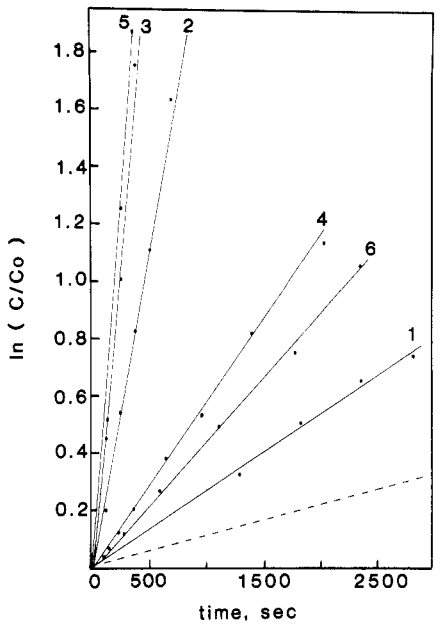

Figure 10. First-order plots for the photooxidation of sulfite for (1) α-FeOOH; (2) γ-Fe_2O_3; (3) α-Fe_2O_3; (4) δ-FeOOH; (5) γ-FeOOH; (6) β-FeOOH. The dashed line is the for dark reaction.

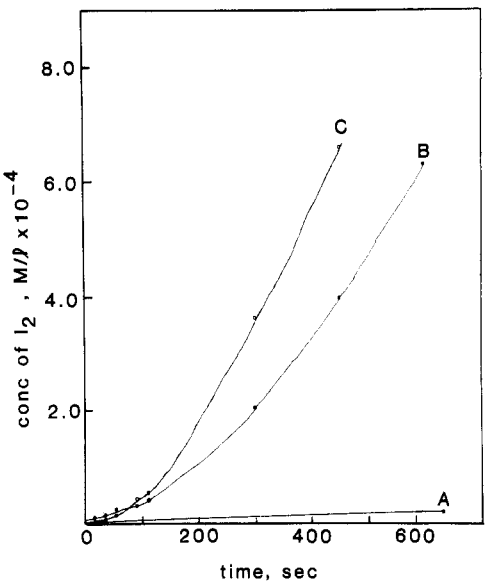

Figure 11. Time dependence of iodine formation for (A) room light and no iron oxide; (B) Xe light with long-pass 300-nm filter and α-Fe_2O_3; (C) Xe light with long-pass 300-nm filter and no iron oxide.

solutions. This can be attributed, again, to the higher pH of the sulfite experiment and the fact that sulfite is a much weaker complexing agent for Fe(II).

The large variation of photooxidation rates demonstrated in the oxalate and sulfite experiments for the different forms of iron oxide is attributed to differences in electronic and structural properties, because there is no correlation between these rates and the hydrodynamic diameter, band gap, or BET surface areas, as shown in Table I. The photooxidation of sulfite by FeO_x/SiO_2 is also first order, and the rate constant (Table I) is of comparable magnitude to the other iron oxides.

The photooxidation of cyanide (pH 12.0) in O_2-saturated solutions with the iron oxides was attempted, but after 6 h of irradiation (1500-W Xe lamp) no oxidation of cyanide occurred. This finding is in agreement with that reported previously on α-Fe_2O_3.[20b] Platinization of the iron oxide particles had no effect. Similarly, no photooxidation of iodide at pH 6.0 (phosphate buffer) in O_2-saturated solution was found after 6 h of illumination. Platinization of the iron oxide particles had no effect. The photooxidation of iodide occurs at pH 1.0 (unbuffered nitric acid

or a phosphate buffer), but the rate is nearly the same in the absence of iron oxide (Figure 11). Note that this reaction is not first order. The homogeneous reaction of O_2 with iodide at this pH occurs readily and is promoted by normal room light. These results differ with those reported previously,[3a] where α-Fe_2O_3 was said to oxidize iodide with large quantum yields. Our conditions were somewhat different, however. Our measurements involved a xenon light with a 300-nm-long pass filter and a longer irradiation time. Moreover, the nature of the electron acceptor in the previous study was not indicated.

Conclusions

The iron oxides show large variations in nE_F*, which are attributed to different surface properties and crystal structure. The et process in these mediation experiments occurs under kinetically controlled conditions.

A model for direct electron transfer from a particle to an electrode was derived to explain the current transients obtained and the log j_{ss} vs. potential behavior. The model demonstrates how charge collection from a particle is affected by recombination, electron transfer, hole transfer, and generation rates. The k^0 values measured for the iron oxides show a wide variation and are generally very small. They can be increased by platinization. The intensity dependence of the steady-state photocurrent suggests extensive e^-/h^+ recombination. Further evidence for this is seen in the numerical solutions for the photocurrent transients. Here, recombination must be much faster than hole transfer to attain a steady-state photocurrent.

The rates of photooxidation of oxalate and sulfite were found to vary by about 2 orders of magnitude with the different iron oxides. This appears to be due to intrinsic differences in crystal and surface structure rather than differences in surface area, hydrodynamic diameter, or band gap.

Acknowledgment. We gratefully acknowledge the support of the National Science Foundation (CHE8304666). We thank Dr. H. Hartman for the iron oxide samples, Professor W. E. Rudzinski for his advice about preparing the FeO_x/SiO_2, and J. Cook for help in setting up the photon correlation spectroscopy measurements.

Electrochemical Investigation of the Electron-Transfer Kinetics and Energetics of Illuminated Tungsten Oxide Colloids

Jonathan K. Leland and Allen J. Bard*

Department of Chemistry, University of Texas, Austin, Texas 78712 *(Received: November 24, 1986; In Final Form: May 19, 1987)*

Electrochemical charge collection techniques were used to study the effects of platinization and reduction on the electron-transfer (et) kinetics and energetics of illuminated tungsten oxide colloids. From the mediated charge collection experiments, the quasi-Fermi level for electrons, nE_F*, was found to be +0.33 V vs. NHE (pH 0) for WO_3 and shifted to +0.21 V for the reduced (H_xWO_3) and platinized (Pt/WO_3) tungsten oxides. The platinization of WO_3 also caused it to be irreversibly reduced. Silica particles coated with a monolayer of WO_3 displayed an nE_F* which was 170 mV negative of that for WO_3. The photocurrent transients for direct et to a collector electrode were potential dependent and were used to measure k^0, the standard heterogeneous rate constant for et, by using a previous treatment derived for iron oxides. The reduction of WO_3 decreased k^0, while platinization slightly increased it.

Introduction

We report here an investigation of the kinetics of direct electron transfer (et) from a WO_3 particle to an electrode in solution, using charge collection techniques.[1] Previously, a model for direct et was developed with iron oxide particles.[2] Here, we apply those concepts to WO_3 to study the effect of platinization and tungsten bronze formation on the et kinetics and compare the properties of WO_3 to those of the iron oxides.[2] Values for nE_F*, the quasi-Fermi level for electrons under illumination, were measured by mediated charge collection techniques.[1a,b] This level in particles is analogous to the flat-band potential for n-type semiconductor electrodes and is a measure of the reducing power of photogenerated electrons in semiconductor colloids and particles. A silica particle coated with a monolayer of WO_3 was prepared for study. This material should mimic a small particle semiconductor colloid with less bulk electron/hole (e^-/h^+) recombination.

As light-collection systems, semiconductor colloids offer some desirable properties.[3] Their small particle diameter affords a high surface area, which is needed for efficient electron and hole transfer to solution and surface species. The heterogeneous rate constants that characterize such reactions for semiconductors are often lower than those for noble metals,[3d] thus necessitating a large surface area to increase the overall rate. Their small diameter allows both charge carriers generated in the bulk to diffuse to the surface before recombination.[3b] This type of behavior makes each particle operate like a miniature photoelectrochemical cell.[3a]

The photoelectrochemistry of single-crystal and polycrystalline WO_3 electrodes has been studied extensively,[4] and WO_3 has also been investigated as an electrochromic material.[5] Kransnovskii

(1) (a) White, J. R.; Bard, A. J. *J. Phys. Chem.* **1985**, *89*, 1947. (b) Ward, M. D.; White, J. R.; Bard, A. J. *J. Am. Chem. Soc.* **1983**, *105*, 27. (c) Ward, M. D.; Bard, A. J. *J. Phys. Chem.* **1982**, *86*, 3599. (d) Bard, A. J.; Pruikisma, R.; White, J. R.; Dunn, W.; Ward, M. D. *Proc. Electrochem. Soc.* **1982**, *82-3*, 381.

(2) Leland, J. K.; Bard, A. J. *J. Phys. Chem.*, accompanying paper in this issue.

(3) (a) Bard, A. J. *J. Photochem.* **1979**, *10*, 59. (b) Curran, J. S.; Lamouche, D. *J. Phys. Chem.* **1983**, *87*, 5405. (c) Fendler, J. H. *J. Phys. Chem.* **1985**, *89*, 2730. (d) Hodes, G.; Grätzel, M. *Nouv. J. Chim.* **1984**, *8*, 509. (e) Bard, A. J. *J. Phys. Chem.* **1982**, *86*, 172. (f) Gerischer, H. *J. Phys. Chem.* **1984**, *88*, 6096.

(4) (a) Reichman, B.; Bard, A. J. *J. Electrochem. Soc.* **1979**, *126*, 2133. (b) Spichigar-Ulmann, M.; Augustynski, J. *J. Appl. Phys.* **1983**, *54*, 6061. (c) Di Quarto, F.; Paola, A.; Sunseri, C. *Electrochim. Acta* **1981**, *26*, 1177. (d) Gerrard, W. A. *J. Electroanal. Chem. Interfacial Electrochem.* **1978**, *86*, 421. (e) Hodes, G.; Cahen, D.; Manassen, J. *Nature (London)* **1976**, *260*, 312. (f) Gissler, W.; Memming, R. *J. Electrochem. Soc.* **1977**, *124*, 1710. (g) Butler, M. A. *J. Appl. Phys.* **1977**, *48*, 1914. (h) Butler, M. A.; Nasby, R. D.; Quinn, R. K. *Solid State Commun.* **1976**, *19*, 1011.

(5) (a) Deb, S. K. *Philos. Mag.* **1973**, *27*, 801. (b) Reichman, B.; Bard, A. J. *J. Electrochem. Soc.* **1979**, *126*, 583. (c) Nogai, J.; Kamimori, T.; Mizuhashi, M. *Rep. Res. Lab. Asahi Glass Co., Ltd.* **1983**, *33*, 99.

0022-3654/87/2091-5083$01.50/0